

Bloch oscillations and resonant Zener tunneling of light in optical superlattices

M. Ghulinyan^a, R. Sapienza^b, C. Toninelli^b, C.J. Oton^c, P. Costantino^b, Z. Gaburro^a, L. Pavesi^a, and D.S. Wiersma^b

^aDipartimento di Fisica, University of Trento, Povo (Trento), Italy

^bEuropean Laboratory for Nonlinear Spectroscopy, Sesto Fiorentino (Florence), Italy

^c Departamento de Fisica Basica, University of La Laguna, Tenerife, Spain

ABSTRACT

We report on optical analogues of well-known electronic phenomena such as Bloch oscillations and electrical Zener breakdown. We describe and detail the experimental observation of Bloch oscillations and resonant Zener tunneling of light waves in static and time-resolved transmission measurements performed on optical superlattices. One-dimensional photonic structures of high optical quality are specifically designed to represent a tilted photonic crystal band. This allows an ultrashort light pulse to bounce between the tilted photonic band edges and hence to perform Bloch oscillations. When the tilt of photonic bands reaches a critical value, two minibands couple within the superlattice structure, resulting in a resonant tunneling channel in the minigap region, where the light transmission boosts from 0.3% to over 43%. The latter case describes the resonant Zener tunneling of light waves.

Keywords: Bloch oscillations, Zener tunneling, optical superlattice, porous silicon

1. INTRODUCTION

Transport phenomena of charge carriers in solids have been studied intensively by the researchers. The energetic spectrum of a quantum particle in a semiconductor crystal consists of allowed and forbidden bands. In the momentum space an electron moves in the allowed energy band running its quasi-impulse in the Brillouin zone. With a given energy, in the real space it travels freely through the infinite crystal. If an external bias is applied on the crystal, the electron is accelerated by the field F in the first half of the Brillouin zone, while in the second half it moves against the field. Therefore in the Brillouin zone it performs a periodic motion which can be either described as a Bragg reflection from the energy band edges. This oscillatory motion is known as electronic Bloch oscillations¹ and has a characteristic period of $T_B = h/eFd$ (d is the lattice constant). The energy spectrum of such a particle in a biased crystal is described by the so-called Wannier-Stark ladder (WSL).² The WSL consists of a set of equidistant states, with an energy separation proportional to the inverse of T_B . In general, Bloch oscillations are expected to occur in an arbitrary periodic lattice, in which the translational invariance is broken, as it happens in the biased semiconductor crystal.

The Bloch oscillations are closely related to another phenomenon, known as electrical breakdown or *nonresonant* Zener tunneling,³ which becomes effective as the electric field increases. At high enough electric fields the electron can tunnel to the continuum of states of the upper energy band without gaining extra energy. With the increasing escape probability of the electron to the other energy band the Bloch oscillations are damped strongly. On the other hand, *resonant* Zener tunneling is possible at high electric fields between charge carriers in WSLs.

The experimental study of electronic Bloch oscillations has been an issue for a long time because of the fact that electrons lose their coherence on a time scale, which is much shorter than the oscillation period T_B . The invention of electronic superlattices⁴ opened up new possibilities to study such interference phenomena, which show faster dynamics than the electron decoherence time. This possibility is brought up by the big translational period of the superlattice structure, which implies a smaller Brillouin zone and therefore shorter oscillation

Corresponding author MG: E-mail: mghool@science.unitn.it, Tel: +39 0461 882030
<http://www.science.unitn.it/~semicon/>; <http://www.complexphotonics.org/>

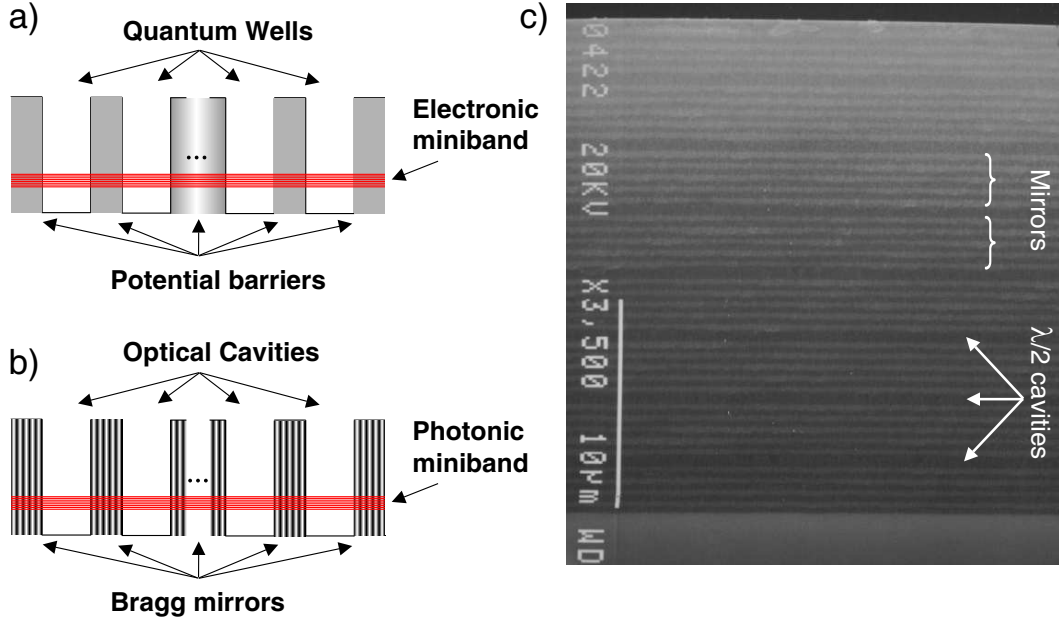


Figure 1. In analogy to the electronic coupling of separate quantum wells in a semiconductor superlattice (a) an optical superlattice can be realized when optical cavities are brought together (b) resulting to the formation of a miniband of extended photonic states. (c) A SEM micrograph of a 1D optical superlattice.

period. Recent experiments cover a series of results such as the observation of WSLs,⁵ Zener breakdown,⁶ and Bloch oscillations.⁷ Resonant tunneling between the anticrossing Wannier-Stark states of neighboring energy minibands has been considered theoretically⁸ and observed in experiments.⁹

The various analogies between the transport of electrons and the propagation of light waves in dielectric materials have been established.¹⁰ Electronic crystals have an analogue in the form of *photonic crystals*. Photonic crystals are artificial materials, in which a periodic variation of dielectric constant leads to the formation of bands where the propagation of photons is allowed or forbidden.¹¹ As the photons do not interact with each other, a light wave packet remains coherent for much longer times than charged particles. This means that dynamic interference effects could be isolated and studied much easier with light.

The existence of the optical counterpart of a WSL has been discussed theoretically¹² and observed experimentally in linearly chirped Moiré gratings.¹³ Different photonic systems have been proposed to observe Bloch oscillations of light waves.^{14,15} Optical superlattices have been proposed as a potentially ideal system to observe Bloch oscillations for light. In these structures an optical path gradient, $\Delta\delta$, *parallel* to the light propagation direction was suggested to mimic the optical equivalent of an external force (the static electric field in the electron case).¹⁶

In this article we report on the observations of optical analogues of electronic Bloch oscillations and electrical Zener breakdown. We will describe and detail the experimental observation of Bloch oscillations¹⁷ and resonant Zener tunneling¹⁸ of light waves in static and time-resolved transmission measurements performed on optical superlattices. In these studies the multilayer structures were specifically designed to represent a tilted photonic crystal band in close analogy to the tilted electronic miniband of a biased semiconductor superlattice. A controlled optical path gradient along the growth direction of the structure causes the formation of an optical Wannier-Stark ladder of equidistant photonic states. The frequency separation of these localized states defines the period of the photon Bloch oscillations. At a critical optical path gradient, we observe resonant coupling of two Wannier-Stark ladders leading to delocalization of the optical waves and hence resonant Zener tunneling.

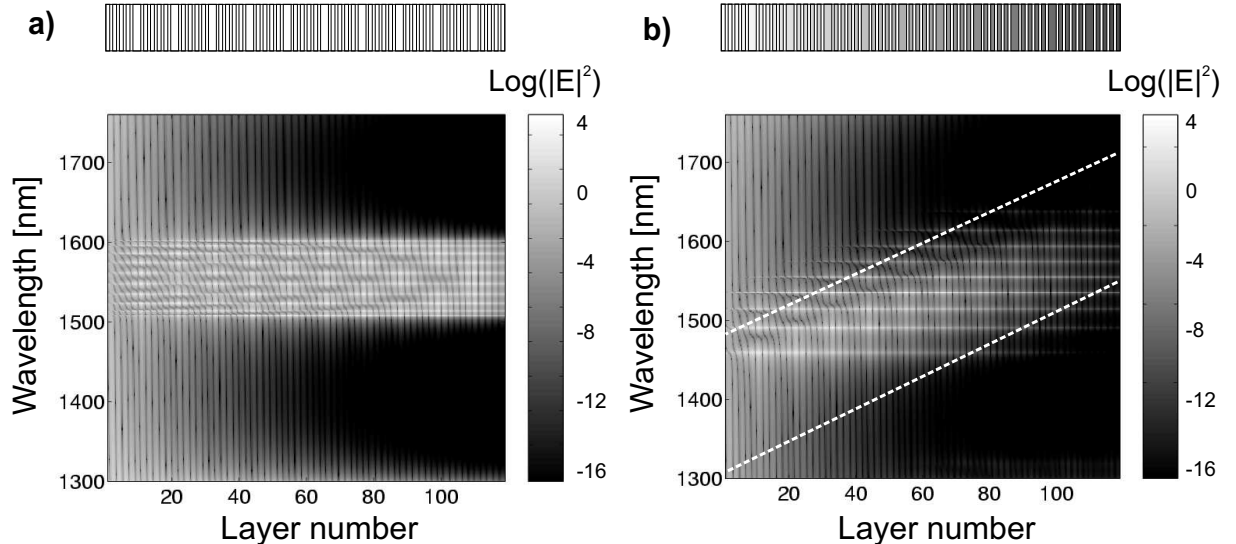


Figure 2. Light intensity distribution inside the optical superlattice structure. The parameters used in the calculations correspond to samples used in the actual experiment. (a) Flat band situation, $\Delta\delta = 0\%$, (b) tilted band situation, $\Delta\delta = 14\%$. The dashed lines are a guide to the eye that indicates the theoretical tilting of the miniband. Above each panel the coupled microcavity structure is schematically shown; the grey scale refers to the refractive index variation along the depth in the sample (the darker the larger n).

2. BLOCH OSCILLATIONS OF LIGHT

2.1. The optical superlattice

In a close analogy to the formation of an electronic superlattice when several semiconductor quantum wells are brought together (Fig. 1(a)), an optical superlattice is made by coupling degenerate optical resonators (cavities) within the same photonic structure (Fig. 1(b)).¹⁹ Optical coupling between the various cavities yields a degenerate mode repulsion²⁰ and a formation of a miniband of optical states, which are densely packed around the resonant wavelength. In one dimension an optical superlattice can be formed by stacking two dielectric layers A and B with different refractive indices and quarter-wave thickness in a way to form identical cavities separated by Bragg reflectors (Fig. 1(c)). In particular, we choose the following sequence of layers: $BABABABAB (AA)_1 BABABABAB (AA)_2 \dots (AA)_m BABABABAB$. This structure is essentially a series of m microcavities $(AA)_m$ coupled to each other through the $BABABABAB$ Bragg reflectors.

The light intensity distribution inside this structure can be calculated using a transfer matrix (TM) formalism.²¹ Figure 2(a) shows the appearance of a miniband of extended optical states (bright lines) in the photonic stop band (dark regions) in the conditions of a unique optical path throughout the structure.

In order to obtain optical Bloch oscillations one has to introduce a gradient in the optical thickness of the layers. This will result in a spatial tilting of the miniband (Fig. 2(b)) and formation in an optical Wannier-Stark ladder. The latter manifests itself as a series of narrow equidistant transmission peaks with a frequency separation of the peaks that defines the period T_B of the Bloch oscillations. The linear change of the optical thickness introduces, to first order, a linear tilt of the miniband.²² The oscillation period will decrease with increase in the miniband tilting.

2.2. Sample preparation and optical WSLs

We have grown the optical superlattices by controlled electrochemical etching of heavily doped p-type (100)-oriented silicon. The electrolyte was prepared mixing a 30% volumetric fraction of aqueous HF (48 wt.%) with ethanol. A magnetic stirrer was used to improve electrolyte exchange. The applied current density defined the porosity of the layer (the latter is related to the effective refractive index of the layer in terms of the Bruggeman

formulae). We applied 7 mA/cm^2 for the low porosity layer A (refractive index $n_A = 2.1$) and 50 mA/cm^2 for the high porosity layer B ($n_B = 1.4$). The physical thickness of the layers was controlled by adjusting the duration of the etch times. Alternating these currents, we grew a superlattice structure with ten coupled cavities. The superlattice structures were made free-standing by applying an electropolishing current pulse at the end of the growth process.¹⁹ The availability of free standing samples is essential to maintain almost excellent control over the growth parameters and further simplified time resolved transmission measurements with no contribution from the strongly absorbing silicon substrate. Particular care was taken to control the anodization conditions which usually drift as the total sample thickness increases. Moreover, the natural refractive index drift was compensated by changing the etching times of the layers. The process is known to provide excellent control over the layer properties allowing the growth of Fabry-Perot filters with a resonance quality factors of 3300.¹⁹

The one dimensional translational symmetry of the superlattice was broken by introducing a optical path gradient in the growth direction of the structure. This was achieved by changing the duration of the etch stop current, which controlled the refractive index and hence the variation in the optical thickness of each layer. We produced samples with gradient values in the range from $\Delta\delta = 2$ to 14% (values that were extracted from the best fit parameters to the transmission spectra). As porous silicon samples suffer from lateral inhomogeneities due to doping variations of the silicon wafers, an inhomogeneous widening of the transmission peaks is usually measured when broad probe beams are used. In order to avoid this some spectra were measured in a high-resolution transmission setup with a very small numerical aperture ($\text{NA} \sim 0.0075$, leading to a negligible broadening of 0.02 nm at 1550 nm wavelength), where a tunable laser source focused to a $35\mu\text{m}$ diameter spot was used.

Figure 3 shows the transmission spectra for different values of gradient $\Delta\delta$. The flat miniband situation is reported in the top panel (Fig. 3(a)). Optical WSLs are formed with an increase in the gradient over a certain value: the bigger is $\Delta\delta$, the larger is the energy separation of the Wannier-Stark states. The resonances become thinner and less intense for the large gradient values (Fig. 3(b-d)). This is a clear signature of the strongly inclined miniband, which also means that in order to be transmitted the photons now need to overcome a thicker tunnelling barrier.

2.3. Time-resolved transmission measurements

We have performed time-resolved transmission experiments on these samples using an optical gating technique. This technique involves mixing a reference beam together with the transmitted signal in a 0.3mm thick non-linear crystal (β Barium Borate) to produce a sum frequency signal. The probe beam is obtained from an optical parametric oscillator (Spectraphysics OPAL) pumped by a Ti:sapphire laser at center wavelength 810 nm (pulse duration 130 fs , average power 2.0 W , repetition rate 82 MHz) yielding short pulses tunable from 1300 to 1600 nm wavelength range (average power 100 mW). The reference pulse at 810 nm wavelength is obtained from the residual Ti:sapphire beam (450 mW average power). The sum frequency signal is detected by a photodiode, and a standard lock-in technique is used to suppress noise. A delay line in the reference beam allows to tune the time delay between signal and reference and thus to scan the signal pulse in time. In the top panel of Fig. 4 we plot the system response without sample from which we determine that the temporal resolution of our system is smaller than 250 fs . The apparatus is designed such that the transmission spectrum of the sample can be monitored during the time-resolved measurement by sampling the transmitted light.

Time-resolved data indeed show that transmitted signals oscillate with a period T_B that decreases as the band tilting increases (Fig. 4). It is important to note that the optical WSL in our structures is formed above a threshold gradient value (7%). This is confirmed also by the TM-calculations. The reason for this is because the optical thickness gradient values below 7% is not sufficient to fully tilt the miniband within the sample thickness. One can see how the amplitude of the transmitted intensity decreases as the gradient increases: as a result of an increased tilt of the photonic miniband (Fig. 2(b)) the oscillating photon wave packet has to tunnel out through a thicker barrier. In Fig. 5 the measured periods of the Bloch oscillations are compared to the ones calculated through TM formalism. The experimental data are in perfect agreement with the theoretical prediction. However, one can measure oscillations even below the critical gradient value of 7% , which in this case are due to the reflection of light from the sample physical boundaries, therefore changing the gradient in this range does not influence the oscillation period. At larger values of gradient the oBO period decreases linearly with the increase in the miniband tilt, as expected for Bloch oscillations.

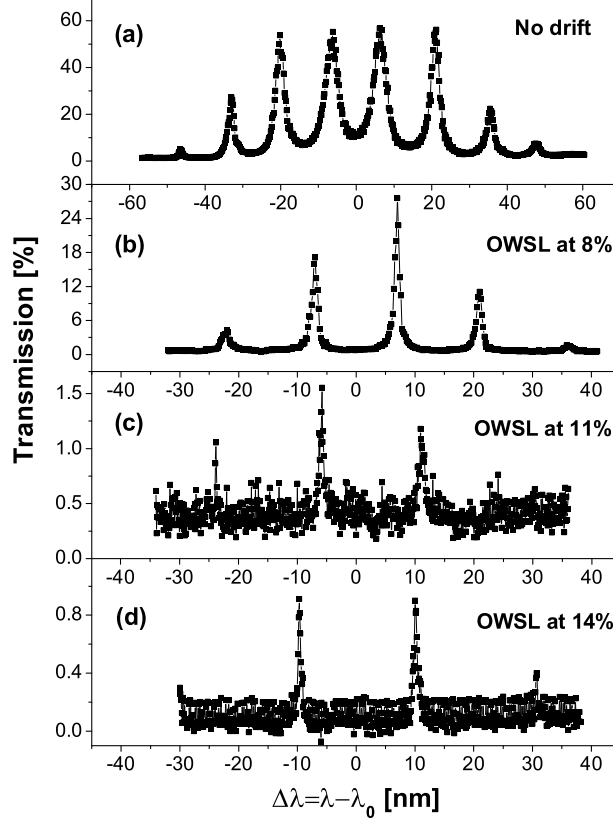


Figure 3. High resolution transmission spectra of the optical superlattices with different gradients of the optical thickness of the layers ($\lambda_0 = 1.55\mu\text{m}$ is the central wavelength). The top spectrum corresponds to the non drifted sample (spatially flat miniband), while the others (b), (c), (d) show the occurrence of the optical Wannier-Stark ladder with equidistant resonances: the energy separation of the states increases with the increase of the miniband tilt.

The oBO decay with a characteristic time τ_B which saturates at large gradients. This is a sign of the increased confinement of the optical modes in the WSL: as the photonic band tilt gets steeper, tunneling out of the sample becomes more difficult, and the transmission losses decrease accordingly. These intrinsic losses are not the only one present in the structure, as light in porous silicon suffers also from external losses. At large gradient values τ_B saturates to 1.26 ps, which is caused by scattering on the pores and residual absorption losses in the porous silicon sample. One can consider that $\tau_B = (\tau_{pBO}^{-1} + \tau_{ext}^{-1})^{-1}$, where τ_{pBO} is the intrinsic decay time of the Bloch oscillation and τ_{ext} is due to absorption and scattering losses. The solid line in Fig. 5 is obtained by assuming $\tau_{ext} = 1.3$ ps that corresponds to an extinction coefficient (total losses, absorption + scattering) of $\alpha_{ext} = 100$ cm⁻¹, in agreement with previously determined loss values.¹⁹

3. RESONANT ZENER TUNNELING OF LIGHT

3.1. The double-miniband optical superlattice

The successful demonstration of the optical analogue of electronic Bloch oscillations naturally raises the question if it is possible to observe the optical analogue of Zener breakdown phenomenon. As a first reasoning towards the study of Zener tunneling of light one should think of tilting the optical superlattice bands such that the first order (centered at λ_c) miniband is coupled to the closest order one. However, very large band tilting will be necessary to do this. A possible solution is to build an optical superlattice that exhibits two minibands within

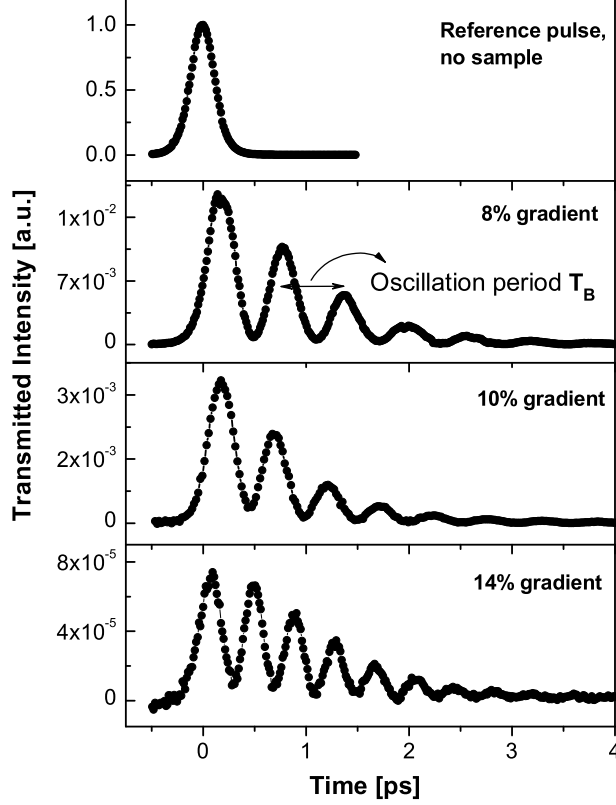


Figure 4. Time-resolved transmitted signals through the superlattice structures for various values of the optical path gradient $\Delta\delta$. The top panel shows the undisturbed probe pulse without sample. An oscillating signal is measured in the photodetector when the optical WSL are excited. The period of the oscillations and the total transmission decrease while increasing $\Delta\delta$.

the unique stop band. This will allow to use relatively small optical path gradients. For this, one should couple within the same structure two sets of cavities of C and D type, which are centered at different wavelengths λ_1 and λ_2 , respectively*. The appropriate sequence of layers looks like the following: $BABABAB (CC)_1 BABABAB (DD)_1 \dots (CC)_m BABABAB (DD)_m BABABAB$. In our studies we have chosen $m=6$, $\lambda_1 = 0.81\lambda_c$ and $\lambda_2 = 0.88\lambda_c$.

The samples were grown using the same technique described in the previous section. The refractive indices for this type of structures were determined to be $n_A = n_C = n_D = 1.5$ and $n_B = 2.12$. We produced samples with controlled gradient values in the range from $\Delta\delta = 0$ to 18%. The light intensity distribution inside this structure in the absence of optical path gradient (Fig. 6(a)) shows the formation of two flat minibands MB1 and MB2. These appear as two sets of intense lines of extended optical states, stretching through the sample. The two minibands are separated by a photonic minigap (dark region), which shows a negligible transmission of 0.43%. The parameters used in the calculations correspond to those of the samples studied in the actual experiment. The calculated spectra also take into account the loss coefficient of 93 cm^{-1} of the samples (due to absorption and scattering out of the propagation axis) which gives a nearly negligible spectral broadening of the transmission peaks of 0.3 – 0.5 nm. The corresponding calculated transmission spectrum of the structure (Fig. 6(b)) is compared with the experimental one (Fig. 6(c)). The latter is measured with a Varian Carry spectrophotometer using a broad beam of 1mm in diameter, which explains appearance of wider and less intense spectral features.

*Note that C and D layers are also quarterwave-thick, so that (CC) and (DD) form $\lambda_1/2$ and $\lambda_2/2$ cavities respectively.

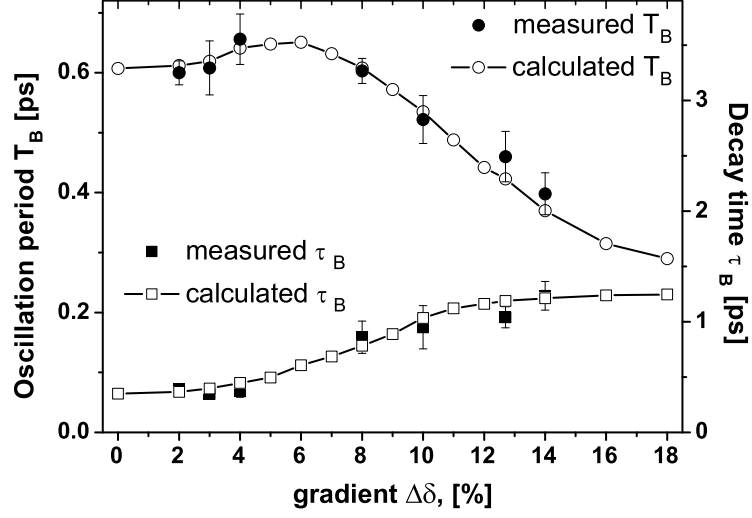


Figure 5. Measured photonic Bloch oscillation period T_B and decay time τ_B as a function of the gradient $\Delta\delta$. The error bars are the standard deviations obtained from various measurements on several positions on the sample and represent therefore the effect of lateral sample inhomogeneities. The solid lines are the predicted from transfer matrix calculations behaviors of T_B and τ_B [*** MODIFY THE CAPTIONS ***].

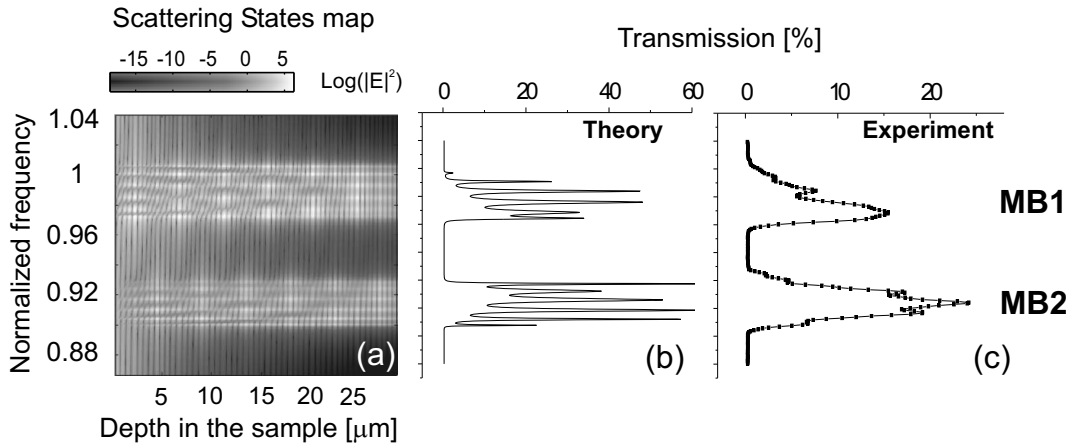


Figure 6. The calculated intensity distribution of the light inside the sample plotted as a color scale versus the normalized frequency ω/ω_0 , where ω_0 is the minigap central frequency, and depth inside the sample. (a) Flat miniband situation, $\Delta\delta = 0\%$. Two minibands MB1 and MB2, separated by a minigap region are seen in the calculated (b) and measured transmission spectrum (c).

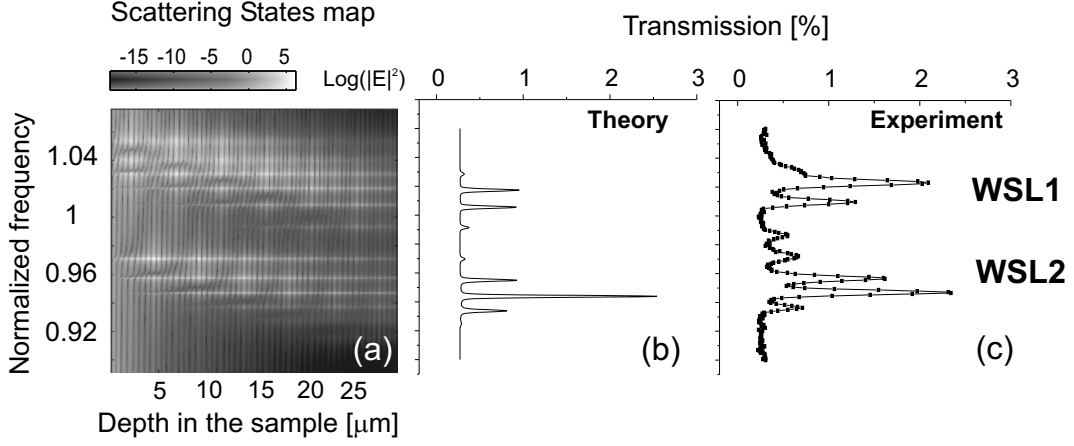


Figure 7. (a) Optical WSLs of localized modes are formed in two minibands at $\Delta\delta = 6.7\%$. Light transmission drops down to 2%: TM-calculations (b) and experiment (c).

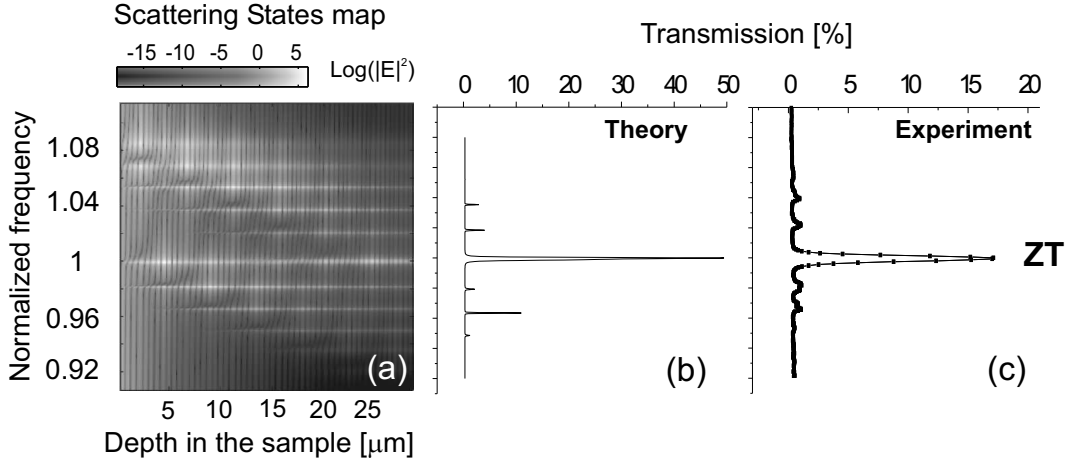


Figure 8. (a) The two WSLs couple at $\Delta\delta = 10.3\%$ and form a resonant tunneling channel through the sample. Resonant Zener tunneling is predicted by theory (b) and confirmed experimentally (c) as an enhanced transmission peak in the center of the minigap.

The high-resolution transmission setup was utilized in some particular cases, where the observation of narrow peaks with high intensity was essential.

An introduction of 6.7% of negative optical path gradient²³ tilts the photonic band structure and results in the formation of optical WSLs in both minibands (Fig. 7(a)). Now the spatial confinement of localized states causes a decrease of absolute transmission from 50% in the flat band case (delocalized states) down to 2% (Fig. 7(b)). In Fig. 7(c) we plot the measured transmission spectrum of the superlattice with tilted minibands, where the WSLs can be appreciated.

We go on further with increasing the optical path gradient and look at the evolution of photonic miniband picture. At a *critical* degree of band tilting ($\Delta\delta \sim 10.3\%$ in our case) the WSLs in two minibands couple within the extension of the structure. Coupling induced delocalization of two anticrossing states takes place, which appears as an intense resonant tunneling channel (Fig. 8(a)). The resonant Zener tunnelling manifests as an enhanced transmission peak peak in both calculated (Fig. 8(b)) and measured transmission spectra (Fig. 8(c)).

This observation, together with the TM-calculations in Figs. 6-8, nicely demonstrates the physics of resonant

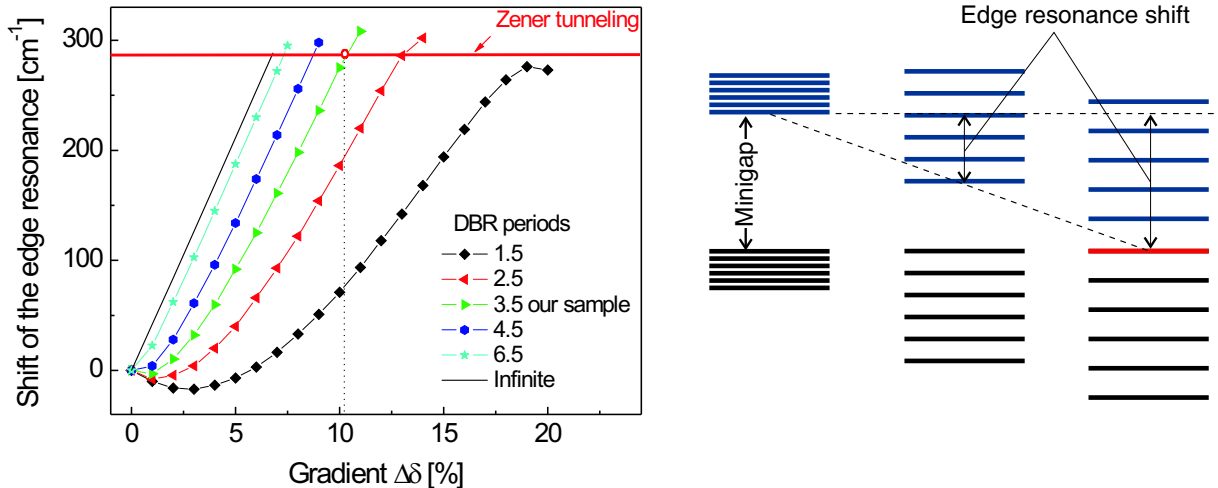


Figure 9. The shift of edge resonance of a miniband relative to its position in the flat band condition. In the limit of very weak coupling between the cavities (solid line) the optical thickness gradient at which Zener tunneling occurs has a minimum value.

Zener tunneling. An efficient transmission channel opens when two internal resonances inside the sample couple to form a delocalized mode of which the transmission coefficient is much larger than the sum of the transmission coefficients of the two individual resonances before coupling. Such internal resonances can only couple if the frequency difference between the modes is smaller than their bandwidth. The characteristic property of Zener tunneling is that this frequency difference is tuned by changing the gradient inside the sample and that the internal resonances arise from a double Wannier-Stark ladder. The critical gradient value $\Delta\delta_{ZT}$ at which Zener tunneling occurs (in our case 10.3%) depends on the frequency difference between the centers of the minigaps $\Delta\omega = \omega_1 - \omega_2$, and the bandwidth of the minibands themselves. At $\Delta\delta_{ZT}$ the frequency of the low frequency miniband at the last cavity (high depth) matches the frequency of the high frequency miniband at the first cavity (small depth). In Fig. 9 we show some numerical results which reflect the evolution of the optical WSLs towards the eventual coupling: the shift of the edge resonance relative to its position in the flat miniband case is plotted versus the increasing $\Delta\delta_{ZT}$. The calculations are performed for different strengths of Bragg mirrors (number of mirror periods) in the optical superlattice. In the limit of very small bandwidth (Bragg mirrors consisting of large number of layers resulting in weak coupling between the cavities) the optical thickness gradient at which Zener tunneling occurs takes its minimum value defined as $\Delta\delta_{ZT} = \Delta\omega/\omega_1$ (solid line). At larger bandwidths the situation is more complicated and to obtain $\Delta\delta_{ZT}$ one needs to calculate the scattering states map at each gradient value as in Fig. 2. We will see below that the such obtained theoretical value for $\Delta\delta_{ZT}$ is indeed 10.3% for our sample.

We can observe from the graph that for the case of strong coupling between the cavities (1.5- and 2.5-period cases) the relative shift of the resonance is negative for small gradients. This is due to the fact that the bandwidth of the miniband decreases slightly when the small gradient detunes only the coupling mirrors but is still not enough to break the translational symmetry of the superlattice. Over a certain value WSLs start to form and the minibands start to expand monotonically with the further increase of titling. Another interesting observation is the behavior of the curve of strongest coupling case (1.5-periods) in the vicinity of $\Delta\delta_{ZT} \approx 18\%$: the coupling between the two WSL states is so strong that the change in the tilting of the miniband around $\Delta\delta_{ZT}$ does not influence the relative shift of the resonance. This means that a marked double peak would manifest in the transmission spectrum for all this range of gradients because of enhanced level repulsion between the degenerate states.

We decided to examine the Zener tunneling regime in detail. For this we have grown a superlattice structure with *lateral* (in-plane) variation in $\Delta\delta$ around 10.3%. To achieve this, the magnetic stirrer was placed close to

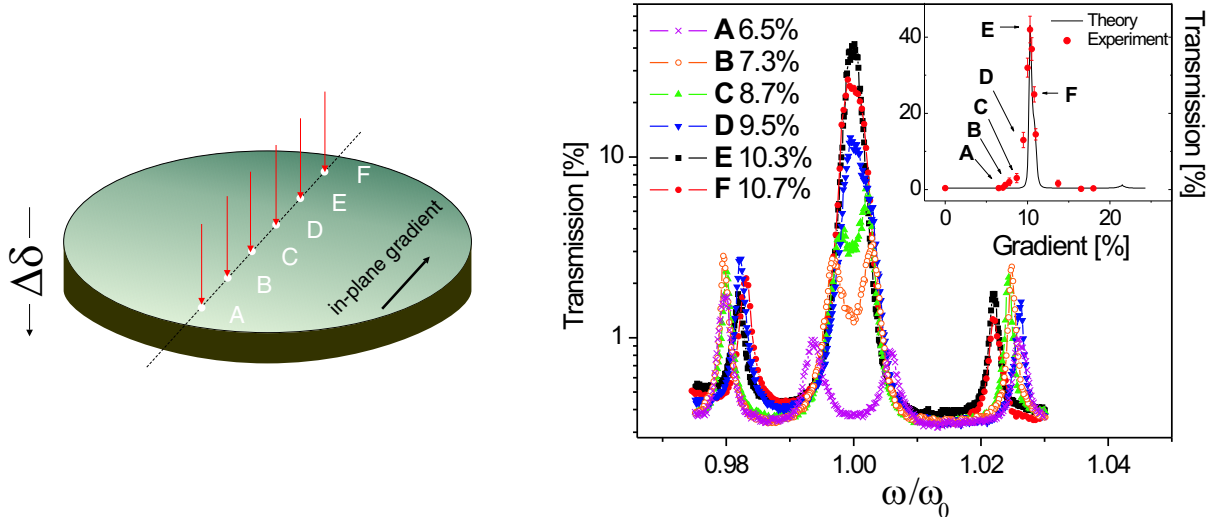


Figure 10. (left) A schematic view of the Hi-Res transmission measurement of the superlattice sample with in-plane gradient. (right) The comparison between the experimental transmission values of the maximum transmission (line) around the central frequency ω_0 as a function of the gradient and the transfer matrix calculations (dots). The inset shows the transmission spectrum of the tilted superlattice around the value of the optical path gradient where the first anti-crossing of the optical Wannier-Stark ladders and hence Zener tunneling occurs.

one edge of the sample during the whole growth process, thus the electrolyte exchange was enhanced differently between the closest (to the stirrer) and farthest points on the sample surface. The latter resulted in a smoothly varying refractive index profile between the antipodal points in each layer of the optical superlattice (see the schematic sketch in Fig. 10). Measuring the transmission spectrum at different points over the sample surface (moving the incident beam laterally) allowed us to follow the evolution of miniband coupling around $\Delta\delta_{ZT}$. In this way the system was studied at different values of gradient between 6.5% to 10.7%.

High-resolution transmission measurements are performed for this sample. Fig. 10 reports the measured high-resolution transmission spectra taken at different points corresponding to different gradients. In the vicinity of the threshold gradient the transmission spectrum is very sensitive to small changes of the optical path. One can see how the edge states of the two WSLs start to overlap, and the saddle-like curvature transforms gradually into a sharp resonance of 42% transmission. In the inset of Fig. 10 the calculated transmission values at ω_0 for $\Delta\delta$ in the range $0 \div 25\%$ are compared with the experimental data. The correspondence between the experimental and calculated values of the Zener tunneling gradient is very good. In the calculations another maximum, corresponding to the second anticrossing of WSL states, is present at $\sim 21\%$. However, the intensity of this peak is much weaker in compare with the first one at $\Delta\delta_{ZT} = 10.3\%$, which can be understood in terms of decreasing the probability of the tunneling event out of the superlattice as the miniband tilt increases.

The analysis of spectra around the Zener tunneling regime show that, together with the increase of the transmission value, the resonant transmission peak gets wider[†]. At resonance its full width half maximum (FWHM) is about a factor of two larger than that of the uncoupled WSL peaks at $0.98\omega_0$ and $1.025\omega_0$. This broader non Lorentzian lineshape is the effect of repulsion between the two coupled resonances.

3.2. Resonant Zener tunneling in time-domain

When studying narrow spectral features in static transmission measurements one usually is limited by the setup resolution. Therefore, lineshape differences are often difficult to appreciate even in the high precision spectra. Small variations in the frequency domain result in big fluctuations in the time domain. The Fourier

[†]The resonance lifetime, which is inversely proportional to the FWHM, decreases for the coupled states, thus proving additionally the coupling induced delocalization of WSL states in the Zener tunneling regime.

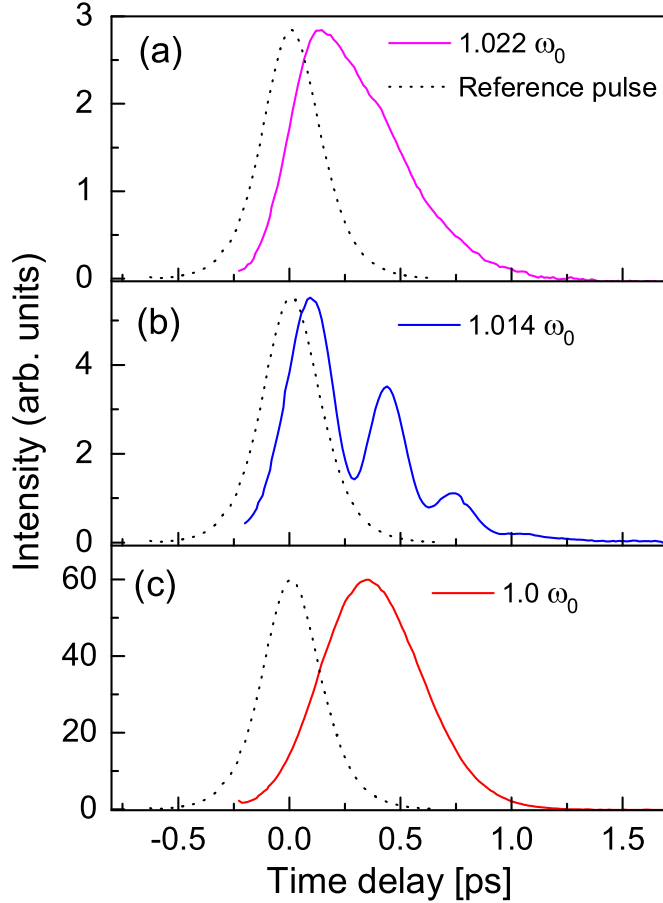


Figure 11. Time-resolved transmitted signals from a double miniband superlattice with optical path gradient in the Zener tunneling regime. The panels (a), (b), and (c) correspond to different probe wavelengths. (a) A excited single resonance shows a characteristic exponential decay whereas (b) damped Bloch oscillations are observed when exciting two Wannier-Stark resonances. In (c) the Zener tunneling peak is excited leading to a strongly delayed but nearly symmetric transmitted pulse. The dotted curves refer to the transmission in the absence of a sample.

transformation of a single resonance, corresponding to a phase shift of π , results in an asymmetric lineshape with single exponential decay at long times. A double resonance mode lineshape (Gaussian) experiences a different phase (2π) versus frequency dependence, which will affect the shape of the time response, namely shifting its maximum towards longer times. Then, the Fourier transformation of a Gaussian peak will result to a more symmetric pulseshape in the time domain. This feature should allow to distinguish among peaks of the same width, originating from resonances of different multiplicity.

We have tested these properties looking at the time response of our optical superlattice sample, performing ultrashort pulse propagation experiment in the Zener tunneling regime. The technique used is the same as described in detail for the Bloch oscillations case. Figure 11 shows three examples of transmitted pulses centered at different wavelengths. A reference pulse, measured in the absence of sample is plotted as dotted line for comparison. When a single Wannier-Stark state is excited (Fig. 11(a)), the transmitted signal intensity decays exponentially, which is the characteristic behavior of a localized state. The delay of the pulse, defined as the delay of the center of the mass of pulse profile, as expected, is not big, because the light propagates only a short region inside the sample, where the resonance is confined. When the incident pulse excites two resonances, a complex signal oscillating with a period of ~ 200 fs, determined by the frequency separation of the excited

states, is observed (Fig. 11(b)). These are the well known photonic Bloch oscillations. In our specific case, these oscillations are damped because of the double resonance acts as an effective a loss channel. Finally, Fig. 11(c) shows the time response of the peak with enhanced transmission at 1560 nm. The time-resolved profile does not have the typical shape of a single resonance. The observed picture is consistent with a double resonance transport behavior: it is characterized by a rapid decay and a substantial delay of maximum transmission point that amounts to almost 360 fs. The fast decay time is due to the strong coupling of the mode with the sample environment. The delay is caused by the transient time necessary to build up the double resonance of the Zener tunneling mode.

4. CONCLUSIONS

In conclusion we have observed the optical counterparts of electronic Bloch oscillations and Zener tunneling in optical superlattices of porous silicon. A linear variation in the optical constants of the system along the propagation direction allows to form a Wannier-Stark ladder and to observe optical Bloch oscillations resolved in time. Both the oscillation period and the damping time versus the strength of the Wannier-Stark ladder are consistent with predictions from transfer matrix calculations. The observation of resonant Zener tunneling of light waves has been performed via spectral and time-resolved transmission measurements on specifically designed optical superlattices, which exhibit two minibands. At a critical gradient of the optical path value, coupling of photonic minibands occurs resulting in delocalization of the optical Wannier-Stark states and consequently Zener tunneling of the light waves.

ACKNOWLEDGMENTS

We wish to thank J.H. Korsch for suggesting the analogy with electronic Zener tunneling and J. Pendry for discussions. This work was financially supported by the INFM projects RANDES and Photonic and by Miur Cofin 2002 and FIRB Sistemi Miniaturizzati per Elettronica e Fotonica and Molecular and Organic/Inorganic Hybrid Nanostructures for Photonics.

REFERENCES

1. F. Bloch, Z. Phys. **52**, 555 (1928).
2. G.H. Wannier, Phys. Rev. **100**, 1227 (1955).
3. C. Zener, Proc. R. Soc A **145**, 532 (1934).
4. L. Esaki and R. Tsu, IBM J. Res. Dev. **14**, 61 (1970).
5. E.E. Mendez, F. Agullo-Rueda, and J.M. Hong, Phys. Rev. Lett. **60**, 2426 (1988).
6. H. Schneider, H.T. Grahn, K.V. Klitzing, K. Ploog, Phys. Rev. Lett. **65**, 2720 (1990); B. Rosam, D. Meinhold, F. Löser, V.G. Lyssenko, S. Glutsch, F. Bechstedt, F. Rossi, K. Köhler, and K. Leo, Phys. Rev. Lett. **86**, 1307 (2001).
7. T. Dekorsy, P. Leisching, K. Köhler, and H. Kurz, Phys. Rev. B **50**, 8106 (1994); V.G. Lyssenko *et al.*, Phys. Rev. Lett. **79**, 301 (1997); T. Hartmann, F. Keck, H. J. Korsch and S. Mossmann, New J. Phys. **6**, 2 (2004).
8. S. Glutsch and F. Bechstedt, Phys. Rev. B **60**, 16584 (1999).
9. B. Rosam, K. Leo, M. Glück, F. Keck, H. J. Korsch, F. Zimmer, K. Köhler, Phys. Rev. B **68**, 125301 (2003).
10. Ping Sheng, *Introduction to Wave Scattering, Localization, and Mesoscopic Phenomena*, Academic Press, New York, (1995); *Wave Scattering in Complex Media, from theory to applications*, edited by S.E. Skipetrov and B.A. van Tiggelen, NATO series II, Vol. **107** (Kluwer, Dordrecht, 2003).
11. J.D. Joannopoulos, R.D. Meade, and J.N. Winn, *Photonic Crystals* (Princeton University Press, Princeton, NJ, 1995); *Photonic Crystals and Light Localization in the 21st Century*, Nato Advanced Research Institute, series C, **563**, edited by C.M. Soukoulis (Kluwer, Dordrecht, 2001).
12. G. Monsivais, M. del Castillo-Mussot, and F. Claro, Phys. Rev. Lett. **64**, 1433 (1990).
13. C. Martijn de Sterke, J.N. Bright, P. A. Krug, and T. E. Hammon, Phys. Rev. E **57**, 2365 (1998).
14. G. Lenz, I. Talanina, and C. Martijn de Sterke, Phys. Rev. Lett. **83**, 963 (1999); A. Kavokin, G. Malpuech, A. Di Carlo, P. Lugli, F. Rossi, Phys. Rev. B **61**, 4413 (2000).

15. P.B. Wilkinson, Phys. Rev. E **65**, 56616 (2002).
16. G. Malpuech, A. Kavokin, G. Panzarini, and A. Di Carlo, Phys. Rev **B 63**, 035108 (2001).
17. R. Sapienza , P. Costantino, D.S. Wiersma, M. Ghulinyan, C.J. Oton, and L. Pavesi, Phys. Rev. Lett. **91**, 263902 (2003).
18. M. Ghulinyan, C.J. Oton, Z. Gaburro, L. Pavesi, C. Toninelli, D.S. Wiersma, Phys. Rev. Lett. **94**, 127401 (2005).
19. M. Ghulinyan, C. J. Oton, G. Bonetti, Z. Gaburro, and L. Pavesi, J. Appl. Phys. **93**, 9724 (2003).
20. L. Pavesi, G. Panzarini, and L.C. Andreani, Phys. Rev. B **58**, 15794 (1998).
21. J.B. Pendry, Adv. Phys. **43**, 461 (1994).
22. Let us consider the flat bandedge energy, $E_0 \sim 1/\lambda_0$ and the tilted bandedge one, $E \sim 1/\lambda$, where $\lambda = \lambda_0(1+\Delta\delta)$, with $\Delta\delta$ the optical path gradient. Then for the ratio $\Delta E/E$ (where $\Delta E = E - E_0$) one can have $\Delta E/E = 1/(1 + \Delta\delta) - 1$, which describes a linear tilt.
23. For technical reasons, the gradient is defined with reference to the last layer. This causes a small shift of the spectral features to higher frequencies when the gradient is increased. A gradient of 6.7% therefore means that the first layer (depth zero) has an optical thickness that is 6.7% smaller than the optical thickness of the last layer.